Crossing the dripline to ^{11}N using elastic resonance scattering

K. Markenroth,[1] L. Axelsson,[1] S. Baxter,[2] M. J. G. Borge,[3] C. Donzaud,[4] S. Fayans,[5] H. O. U. Fynbo,[6] V. Z. Goldberg,[5] S. Grévy,[10] D. Guillemaud-Mueller,[4] B. Jonson,[1] K.-M. Källman,[7] S. Leenhardt,[4] M. Lewitowicz,[8] T. Lönnroth,[7] P. Manngård,[7] I. Martel,[3] A. C. Mueller,[4] I. Mukha,[5,12] T. Nilsson,[6] G. Nyman,[1] N. A. Orr,[10] K. Riisager,[9] G. V. Rogachev,[5,14] M.-G. Saint-Laurent,[8] I. N. Serikov,[5] N. B. Shul'gina,[1,5] O. Sorlin,[4] M. Steiner,[2] O. Tengblad,[3] M. Thoennessen,[2] E. Tryggestad,[2] W. H. Trzaska,[13] F. Wenander,[1,6] J. S. Winfield,[10] and R. Wolski[11]

[1]*Experimentell Fysik, Chalmers Tekniska Högskola och Göteborgs Universitet, S-412 96 Göteborg, Sweden*

[2]*NSCL, Michigan State University, East Lansing, Michigan 48824*

[3]*Instituto de Estructura de la Materia, CSIC, E-28006 Madrid, Spain*

[4]*Institut de Physique Nucléaire, IN2P3-CNRS, F-91406 Orsay Cedex, France*

[5]*Kurchatov Institute, Institute of General and Nuclear Physics, RU-123182 Moscow, Russia*

[6]*EP Division, CERN, CH-1211 Geneva 23, Switzerland*

[7]*Department of Physics, Åbo Akademi, FIN-20500 Turku, Finland*

[8]*GANIL, BP 5027, F-14021 Caen Cedex, France*

[9]*Institut for Fysik og Astronomi, Aarhus Universitet, DK-8000 Aarhus C, Denmark*

[10]*Laboratoire de Physique Corpusculaire, F-14050 Caen Cedex, France*

[11]*Institute of Nuclear Physics, Cracow, Poland*

[12]*Technische Universität, D-64289 Darmstadt, Germany*

[13]*Department of Physics, University of Jyväskylä, JYFL, FIN-40351 Jyväskylä, Finland*

[14]*Department of Physics, University of Notre Dame, Notre Dame, Indiana 46556*

(Received 22 December 1999; published 16 August 2000)

The level structure of the unbound nucleus ^{11}N has been studied by ^{10}C+p elastic resonance scattering in inverse geometry with the LISE3 spectrometer at GANIL, using a ^{10}C beam with an energy of 9.0 MeV/nucleon. An additional measurement was done at the A1200 spectrometer at MSU. The excitation function above the ^{10}C+p threshold has been determined up to 5 MeV. A potential-model analysis revealed three resonance states at energies $1.27^{+0.18}_{-0.05}$ MeV ($\Gamma = 1.44 \pm 0.2$ MeV), $2.01^{+0.15}_{-0.05}$ MeV ($\Gamma = 0.84 \pm 0.2$ MeV), and 3.75 ± 0.05 MeV ($\Gamma = 0.60 \pm 0.05$ MeV) with the spin-parity assignments $I^\pi = \frac{1}{2}^+, \frac{1}{2}^-, \frac{5}{2}^+$, respectively. Hence, ^{11}N is shown to have a ground state parity inversion completely analogous to its mirror partner ^{11}Be. A narrow resonance in the excitation function at 4.33 ± 0.05 MeV was also observed and assigned spin parity $\frac{3}{2}^-$.

PACS number(s): 21.10.Hw, 21.10.Pc, 25.40.Ny, 27.20.+n

I. INTRODUCTION

The exploration of exotic nuclei is one of the most intriguing and fastest expanding fields in modern nuclear physics. The research in this domain has introduced many new and unexpected phenomena of which a few examples are halo systems, intruder states, soft excitation modes, and rare β-delayed particle decays. To comprehend the new features of the nuclear world that are revealed as the driplines are approached, reliable and unambiguous experimental data are needed. Presently available data for nuclei close to the driplines mainly give ground-state properties as masses, ground state I^π, and β-decay half-lives. Also information on energies, widths, and quantum numbers I^π of excited nuclear levels are vital for an understanding of the exotic nuclei but are to a large extent limited to what can be extracted from β decays. Nuclear reactions can give additional information, in particular concerning unbound nuclear systems. However, the exotic species are mainly produced in complicated reactions between stable nuclei. These processes are normally far too complex to allow for spin-parity assignments of the populated states, and hence are of limited use for spectroscopic investigations. Instead of using complex reactions between stable nuclei, the driplines can be approached in simple reactions involving radioactive nuclei. An example is given in this paper where elastic resonance scattering of a ^{10}C beam on a hydrogen target was used to study the unbound nucleus ^{11}N. With heavy ions as beam and light particles as target, the technique employed here is performed in inverse geometry. The use of a thick gas target instead of a solid target is another novel approach. This technique has been developed at the Kurchatov Institute [1] where it has been employed to study unbound cluster states with stable beams [2]. The perspectives of using radioactive beams in inverse kinematics reactions to study exotic nuclei are discussed in Ref. [3] and the method was used in Ref. [4]. Resonance elastic scattering in inverse kinematics using radioactive beams and a solid target has been used at Louvain-la-Neuve [5,6].

This experiment is part of a large program for investigating the properties of halo states in nuclei [7]. A well studied halo nucleus is ^{11}Be where experiments have demonstrated that the ground state halo mainly consists of an $1s_{1/2}$ neutron coupled to the deformed ^{10}Be core [8,9], in contradiction to shell-model which predicts that the odd neutron should be in a $0p_{1/2}$ state. The $0p_{1/2}$ level is in reality the first excited state, while the ground state is a $1s_{1/2}$ intruder level [10]. This discovery has been followed by numerous papers inves-

stigating the inversion, e.g., Refs. [11,12]. The mirror nucleus of ^{11}Be, ^{11}N, should have a $\frac{1}{2}^+$ ground state with the odd proton being mainly in the $1s_{1/2}$ orbit, if the symmetry of mirror pairs holds. However, ^{11}N is unbound with respect to proton emission which means that all states are resonances that can be studied in elastic scattering reactions. The first experiment devoted to a study of the properties of the low-energy structure of ^{11}N used the three-nucleon transfer-reaction ^{14}N(^{3}He,^{6}He)^{11}N. The results indicated a resonant state at 2.24 MeV [13] which was interpreted as the first excited $\frac{1}{2}^-$ state rather than the $\frac{1}{2}^+$ ground state.

In this paper we present excitation functions at laboratory (lab) angles of 0° measured at GANIL [4] and MSU, and at 12.5° with respect to the beam direction measured at GANIL. A thorough analysis, using a potential model as well as a simplified *R*-matrix treatment, gives unambiguous determination of the quantum structure of the three lowest resonances in the ^{10}C+p system.

II. ELASTIC RESONANCE SCATTERING: METHOD AND FORMALISM

The first description of elastic resonance scattering was given by Breit and Wigner [14], and it is now a theoretically well understood reaction mechanism [15,16]. Traditionally, elastic resonance scattering experiments have been performed by bombarding a thin target with a light ion beam, narrow in space and time. To obtain an excitation function the beam energy then had to be changed in small steps of the order of the experimental resolution. The need for a radioactive target severely limits the applicability of this method to investigations in regions close to β stability. However, it is possible to produce dripline species in simple reactions involving radioactive nuclei. When using this approach, the beam is composed of radioactive ions and the target of light nuclei, eliminating the need for a radioactive target. Since this is the inverse setup to the one traditionally used in scattering experiments, the method is usually denoted as elastic scattering in inverse geometry.

The advantage of using gas instead of a solid target is twofold. First, the thickness of a gas target can be changed continuously and easily by adjusting the gas pressure, and secondly the target is very homogeneous. The beam parameters of radioactive ion beams (RIB's) are limited; the spread in both energy and space are much larger than what can be obtained for stable beams, and the intensities are of course much smaller. As will be seen below, the beam properties are not of great importance in the experimental approach used here. Elastic resonance scattering is characterized by large cross sections and is therefore well suited for use with low-intensity RIB's. These and several other features of the elastic resonance scattering in inverse geometry on thick targets will be illuminated in the following subsections.

The expressions for elastic cross section in the case of proton scattering on spinless nuclei, Eqs. (1) and (2), can, for example, be found in Ref. [16],

$$\frac{d\sigma}{d\Omega} = |A(\theta)|^2 + |B(\theta)|^2, \tag{1}$$

where

$$A(\theta) = \frac{zZ}{2\mu v \sin^2(\theta/2)} e^{(i\hbar/\mu v)\ln[1/\sin^2(\theta/2)]} + \frac{1}{2ik}\sum_{l=0}^{\infty}[(l+1)(e^{2i\delta_l^+}-1)+l(e^{2i\delta_l^-}-1)] \times e^{2i\sigma_l}P_l(\cos\theta) \tag{2}$$

and

$$B(\theta) = \frac{i}{2k}\sum_{l=0}^{\infty}(e^{2i\delta_l^+}-e^{2i\delta_l^-})e^{2i\sigma_l}P_l^1(\cos\theta),$$

where $e^{2i\sigma_l}$ is defined by

$$e^{2i\sigma_l} = \frac{\Gamma(l+1+i/k)}{\Gamma(l+1-i/k)}. \tag{3}$$

The symbol $\pm$ denotes states with $j = l \pm 1/2$, z is the proton charge, Z is the charge of the zero-spin particle, and μ is the reduced mass of the system. Further, ν defines the relative velocity between the particles, k is the magnitude of the wave vector, σ_l is the Coulomb phase shift, and $P_l(\cos\theta)$ and $P_l^1(\cos\theta)$ are the Legendre polynomials and associated Legendre polynomials, respectively.

The first term in $A(\theta)$ represents the Coulomb scattering. The other terms in $A(\theta)$ and $B(\theta)$ express scattering due to nuclear forces. The phase shift δ_l is the sum of the phase shift from hard sphere scattering $-\phi_l$ and the resonant nuclear phase shift β_l:

$$\delta_l^+ = \beta_l^+ - g f_l, \quad \delta_l^- = \beta_l^- - \phi_l. \tag{4}$$

The differential cross section has its maximum in the vicinity of the position where the phase shift passes through $(n+\frac{1}{2})\pi$. Therefore, a frequently used definition of the resonance energy is where $\delta = (n+\frac{1}{2})\pi$, see Sec. IV. It is favorable to study resonance scattering at 180° c.m., where Eq. (1) is simplified. At this angle, only $m=0$ substates contribute to the cross section and both potential and Coulomb scattering are minimal. An advantage of the inverse geometry setup is its possibility to measure at 180° c.m.

A. Kinematical relations

We define the laboratory energies of the bombarding particles before the interaction in inverse (E) and conventional (T) geometry as E_0 and T_0, respectively. The notation used mainly follows Ref. [17], primed energies being in the c.m. system. In the following, m and M denote the masses of the light and heavy particles, respectively. E_M and T_M define the laboratory energies of the heavy particle after interaction in the two systems, while E_m and T_m are the analog entities for the light particle. The scattering angle in the laboratory system is written $\theta_{\rm lab}$. The relations between laboratory energy of the beam and the c.m. energy of the heavy nucleus are

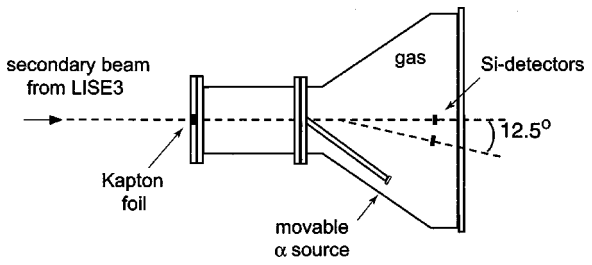

FIG. 1. A schematic view of the scattering chamber and Si detectors. The 12.5° detector has this angle to the middle of the chamber. The interaction position and the corresponding angle are calculated for each event when analyzing the data.

$$T'_M = T_0 \frac{mM}{(M+m)^2} \Leftrightarrow E'_M = E_0 \left(\frac{m}{M+m} \right)^2 . \tag{5}$$

The expressions for the lab energies of the light particle m that will be detected after scattering:

$$T_m = T_0 \left(\frac{m}{M+m} \right)^2 (\cos\theta_{\rm lab} + \sqrt{K^2 - \sin^2 - \theta})^2$$

$$\Leftrightarrow E_m = E_0 \frac{4mM}{(M+m)^2} \cos^2\theta_{\rm lab} . \tag{6}$$

In the equation above, K is the ratio of the masses ($E_0/T_0 = M/m = K$ since $E'_M = T'_M$). Inserting $\theta_{\rm lab} = 0°$ in Eq. (6) leads to the following ratio between the energy of the measured particle in conventional and inverse geometry:

$$\frac{E_m}{T_m} = 4 \frac{K^2}{(1+K)^2} \sim 4. \tag{7}$$

As seen from Eq. (7), the detected energy of the light particles is close to 4 times higher for inverse kinematics as compared to the conventional geometry at the same c.m. energy. This is an important gain for the study of resonant states near the threshold. The excitation energy in the $M+m$ compound system is obtained as the sum of the c.m. energies for particles m and M:

$$T_{\rm ex} = T_0 \frac{M}{M+m} \Leftrightarrow E_{\rm ex} = E_0 \frac{m}{M+m} . \tag{8}$$

Using Eq. (6), this can be expressed in terms of the measured particle energy E_m. In the case of inverse kinematics, the excitation energy of the compound system becomes

$$E_{\rm ex} = \frac{M+m}{4M \cos^2(\theta_{\rm lab})} E_m . \tag{9}$$

Because of the low energies involved, a nonrelativistic expression can be used.

B. General setup of elastic scattering in inverse geometry

The basic experimental setup consists of a radioactive ion beam which is incident on a scattering chamber filled with gas. The thickness of the gas target is adjusted to be slightly greater than the range of the beam ions. Charged-particle detectors are placed at and around the beam direction, i.e., 180° c.m., as shown in Fig. 1. As they are continuously slowed down in the gas, the beam ions effectively scan the energy region from the beam energy down to zero, giving a continuous excitation function in this interval. When the energy of the heavy ion corresponds to a resonance in the compound system, the cross section for elastic scattering increases dramatically and can exceed 1 b, making it possible to neglect the nonresonant contributions which are on the order of mb. For the ideal case of a monoenergetic beam, each interaction point along the beam direction in the chamber corresponds uniquely to one resonance energy and, as we study elastic scattering, to a specific proton energy for each given angle. Because the distance from the detector is different for each proton energy, the solid angle also varies with proton energy and is quite different for low- and high-energy resonances.

The high efficiency of the method is mainly a result of the large investigated energy region. If we compare the scanned region of 5–10 MeV with the typical energy step of ≈10–20 keV in conventional scattering measurements, the gain is 250–1000 times.

C. Energy resolution

The initial energy spread of our ^{10}C beam was 1.5% of the total energy, which naturally increased along the beam path in the gas. The energy spread of the beam results in excitation of the same resonance at different distances from the detector. Assuming that ΔE is the energy spread at some point in the gas, this distance interval Δx is given by

$$\Delta x = \frac{\Delta E}{(dE/dx)M} , \tag{10}$$

where $(dE/dx)_M$ is the specific energy loss of the beam nuclei in the gas. Due to the protons energy loss in the gas, the measured proton energies corresponding to the same resonance are slightly different. The resulting spread of proton energies ε corresponding to the interval Δx will be

$$\varepsilon = \Delta E \frac{(dE/dx)_m}{(dE/dx)_M} . \tag{11}$$

Here, $(dE/dx)_m$ denotes the specific energy loss of the recoil nuclei (protons) in the gas. Taking into account the different velocities of the beam ions and the scattered protons as well as the Bethe-Bloch expression for specific energy loss, one finds

$$\varepsilon \sim \frac{\Delta E}{4} \frac{z^2}{Z^2} . \tag{12}$$

In the case of ^{10}C+p interaction, Eq. (12) becomes $\varepsilon \sim \Delta E/144$. Hence, for $\Delta E = 5$ MeV a lab energy resolution of 35 keV is expected. The effective c.m. energy resolution will be about four times better than the resolution in the lab frame, see Eq. (7). Thus it is clearly shown that the energy spread of the radioactive beam does not restrict the applica-

bility of the method. Many other factors influence the final resolution, for example the size of the beam spot and detectors, the detector resolution, the angular divergence of the beam, and straggling of light particles in the gas. These factors can be taken into account by Monte Carlo simulations. In reality, an effective energy resolution of 20 keV in the c.m. frame is feasible. At angles other than 180° the resolution deteriorates, mainly due to kinematical broadening of the energy signals for protons scattered at different angles. This contribution to the resolution could be reduced by tracking the proton angles.

D. Background sources

A cornerstone of the described experimental approach is that elastic resonance scattering dominates over other possible processes. The competing reaction channel which has to be treated for each specific case is inelastic resonance scattering, as it is a resonant process which produces the same recoil particles as the elastic scattering. However, the elastic and inelastic resonance scattering reactions can be distinguished from each other. The energy of the scattered nuclei from inelastic resonance scattering at 0° is given by Eq. (13) if $E^*/E_0 \ll 1$, where E^* is the excitation energy of the beam nucleus [17]

$$E_m \approx 4 \frac{mM}{(M+m)^2} \left(E_0 - \frac{E^*}{2} \frac{M+m}{m} \right). \tag{13}$$

Comparing this with Eq. (9), one sees that the energy of heavy ions has to be larger by an amount $\mathcal{E}$ for the inelastic scattering to obtain the same energy of a light recoil from the elastic and inelastic scattering reactions, when $\mathcal{E}$ is defined in Eq. (14):

$$\mathcal{E} \approx \frac{E^*}{2} \frac{M+m}{m}. \tag{14}$$

For the $^{10}C+p$ case, where $E^*[^{10}C(2_1^+)]=3.35$ MeV, Eq. (14) shows that the inelastic resonance scattering should take place at about 20 MeV higher energy than the elastic one for the two processes to mix in the elastic scattering excitation function. The inelastic resonance reaction thus has to take place further from the detectors, closer to the entrance window, in order to produce a scattered particle with the same energy as the corresponding elastic process. The two processes in question hence can give the same energies of the recoil protons but their time of flight (TOF) (window-detector) will differ. The time difference between the two types of events will be on the order of a few ns, and can thus be separated in the analysis. No such events were seen in our data.

Other scattering reactions contribute very little to the spectrum, especially at 180° c.m., the exception being low energies where the Coulomb, scattering cross sections increase. However, this scattering is well understood and can be included in the data treatment. Additional sources of background are β particles from decaying radioactive ions in the gas, beam ions which penetrate the gas target, and particles scattered in the entrance window.

III. EXPERIMENTAL PROCEDURE

The first experiment was performed using the LISE3 spectrometer at the GANIL heavy-ion facility. The secondary ^{10}C beam was produced by a 75 MeV/nucleon $^{12}C^{6+}$ beam with an intensity of 2×10^{12} ions/s which bombarded a 8 mm thick, rotating Be target and a fixed 400 μm Ta target. The ^{10}C fragments were selected in the LISE3 spectrometer, using an achromatic degrader at the intermediate focal plane (Be, 220 μm thick) and the Wien-filter after the last dipole. The 50 cm long scattering chamber was placed at the final focal plane. Immediately before the 80 μm thick kapton entrance window, a PPAC (parallel plate avalanche counter) registered the position of the incoming ions. The intensity of the secondary beam, measured by the PPAC, was approximately 7000 ions/s, and due to the degrader and Wien filter a very low degree of contamination was achieved. The efficiency of the PPAC at this intensity and ion charge is close to 100%, which makes it easy to use the PPAC count rate to obtain absolute cross sections. The scattering chamber was filled with CH_4 gas, acting as a thick proton target for the incoming ^{10}C ions. The gas pressure was adjusted to 816 $\pm$5 mbar, which was the pressure required to stop the incoming beam just in front of the central detector. It is desirable to stop the beam close to the detectors in order to avoid loosing any protons scattered from a possible low-lying resonance in ^{11}N. In the far end of the chamber an array of Si detectors was placed. The detectors had diameters of 20 mm and thickness of 2.50 mm, corresponding to the range of 20 MeV protons. The time between the radio frequency (RF) from the cyclotron and the PPAC gave one time-of-flight signal, while the time difference of the PPAC and detector signal gave additional TOF information. The complete setup is shown in Fig. 1.

As a first measurement, a low intensity ^{10}C beam was sent into the evacuated scattering chamber to get the total energy and spread of the secondary beam after the foil, and this was determined to be 90 MeV with a FWHM=1.5 MeV. For background measurements, the scattering chamber was filled with CO_2 gas at 450$\pm$5 mbar and bombarded with ^{12}C and ^{10}C beams, respectively. For our purposes, we assume that ^{16}O and ^{12}C behave similarly in proton scattering reactions. The measurements with the CO_2 target would reveal any background stemming from the carbon nuclei in the CH_4 target gas or from the kapton window. Beam contaminations would also be present in these runs, and those background sources can subsequently be subtracted from the experimental excitation functions.

The standard beam diagnostics observed admixtures of d, α, and ^6Li with the same velocity as the ^{12}C secondary beam, while no contaminant particles could be seen in the ^{10}C beam. The $^{10}C+CO_2$ spectrum showed no prominent structure and was found to contribute less than 10% to the total cross section. This background spectrum was subtracted from the $^{10}C+CH_4$ spectrum before transformation to the c.m. system.

Since ^{10}C is a β^+ emitter with a half-life of 19.3 s, it is necessary to discriminate the positron signals from the protons. This was done by selecting the protons in a two-

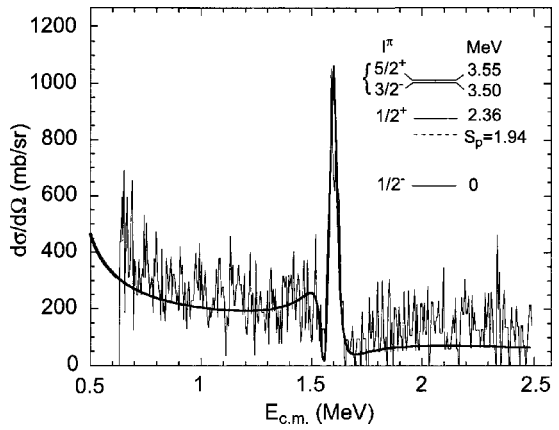

FIG. 2. Experimental spectrum of protons from the scattering of ^{12}C. The energy is given as c.m. energy of ^{13}N. The peaks are fitted with two coherently added resonances as described in the text.

dimensional spectrum showing TOF (PPAC to Si detector) versus detected energy, where the positrons are clearly distinguished from protons both by their uniform time distribution and their maximum energy of 1.93 MeV. A positron with energy in this interval has a maximum energy loss of 1.25 MeV in 2.50 mm Si, which simulates a scattered proton energy of 0.344 MeV in the excitation function of ^{11}N. Since the positron energies are small enough to lie in the energy range of Coulomb scattered protons, cutting away all events below this energy does not distort the interesting parts of the proton spectrum, as is seen in the inset in Fig. 3.

In this paragraph we justify our ignoring the background contributions to our spectra from inelastic scattering of ^{10}C on hydrogen with excitation of the particle stable 2^+ level at 3.35 MeV in ^{10}C. The contribution from inelastic scattering has been estimated using available data on inelastic scattering of protons on a ^{10}Be target [18] and a DWBA extrapolation to the whole investigated interval of energies. This shows that the contribution from inelastic scattering does not exceed 1% of the observed cross section.

The energy calibration of the Si detectors was done with a triple α source (^{244}Cm, ^{241}Am, and ^{239}Pu) which was placed on a movable arm inside the chamber. Another calibration, and at the same time a performance check of the setup, was done by investigating known resonances in ^{13}N. The primary ^{12}C beam, degraded to 6.25 MeV/nucleon, was scattered on the methane target using a gas pressure of 240 ± 5 mbar. The resulting proton spectrum clearly shows the two closely lying resonances in ^{13}N (3.50 MeV, width 62 keV, and 3.55 MeV, width 47 keV [19]), as can be seen in Fig. 2.

These resonances are overlapping and the width of the peak is 50 keV. The solid curve in Fig. 2 is a fit obtained by coherently adding two curves in order to take interference into account. The $\frac{5}{2}^+$ resonance at 3.55 MeV has single particle (SP) nature [19] and was described using the potential model outlined in Sec. IV, while a Breit-Wigner curve was used for the $\frac{3}{2}^-$ state at 3.50 MeV. The resonant $\frac{1}{2}^+$ state in ^{13}N, 420 keV above the $^{12}\mathrm{C}+p$ threshold, is not seen as it is overlapping the Coulomb scattering which dominates below 0.5 MeV. From the calibration measurements described above an energy resolution of 100 keV in the lab frame was

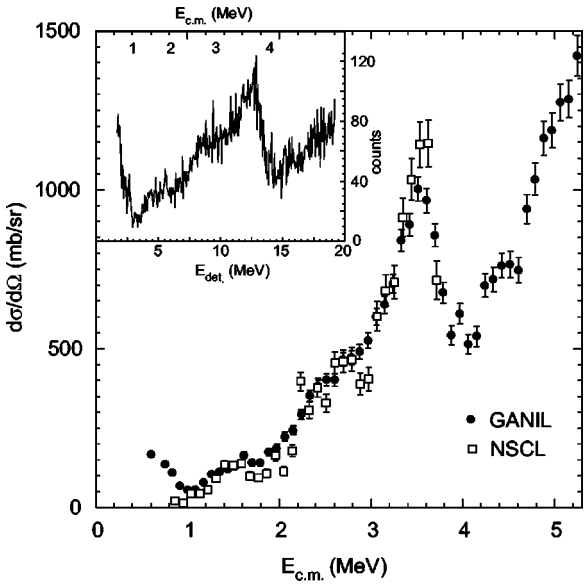

FIG. 3. The excitation function of ^{11}N is shown after background subtraction and transformation to the c.m. system. The filled black circles represent the GANIL data, and the white squares show the result of the MSU experiment. The inset shows the raw data in the lab system. The upper scale in the inset is a rough calibration to c.m. energy, shown for comparison, while the lower scale is the detected proton energy.

deduced, mainly determined by the detector resolutions and proton straggling in the gas.

The experimental proton spectrum was, after subtraction of the measured carbon background, transformed into differential cross section as a function of the excitation energy of ^{11}N, in the following referred to as the excitation function of ^{11}N. Since each interaction point along the beam direction ideally corresponds to a specific resonance energy, the measured proton energy can, after correction for its energy loss in the gas, be used to find the resonance energy in ^{11}N in the c.m. system. The inset in Fig. 3 shows the experimental data as measured proton energy versus counts at 0° before the corrections for solid angle was made. Comparing this pictures to the one obtained after transformation to the c.m. system clearly shows the effect of differing solid angles for different proton energies. The cross sections in the high energy part increases relative to the low energy part, as is clearly seen when comparing the inset to the transformed spectrum in Fig. 3.

Extracting the cross section from the data is straightforward, and the transformation to c.m. is done using Eq. (15):

$$\left(\frac{d\sigma}{d\Omega}\right)_{\mathrm{c.m.}} = \frac{1}{4\cos(\theta_{\mathrm{lab}})}\left(\frac{d\sigma}{d\Omega}\right)_{\mathrm{lab}}. \tag{15}$$

The relation between the scattering angle in the lab and c.m. systems is simply $\theta_{\mathrm{c.m.}} = 180° - 2\theta_{\mathrm{lab}}$. The excitation function obtained after background subtraction and transformation into the c.m. system is shown in Fig. 3. The more de-

tailed analysis now performed revises the absolute cross section to a larger value from what was previously published in Ref. [4].

A second independent measurement of $^{10}C+p$ elastic scattering using the same method was made at NSCL where the A1200 spectrometer delivered the ^{10}C beam. The experimental conditions were the same as in the GANIL experiment, except that at NSCL a ΔE-E telescope was placed at 0° and no Wien-filter was used. The energy of the ^{10}C beam after the foil was 7.4 MeV/nucleon and the beam intensity was 2000 pps. The data from these two experiments are overlaid in Fig. 3 where it is seen that the structures and the absolute cross sections coincide.

IV. ANALYSIS AND RESULTS

The excitation function, shown in Fig. 3, reveals structure in the region from 1 to 4 MeV that could be due to interfering broad resonances. A reasonable first assumption is that the structure corresponds to the three lowest states in ^{11}N. This assumption is justified by the closed proton $p_{3/2}$ subshell in ^{10}C and agrees with the known predominantly single particle nature of the lowest states in ^{11}Be [20], the mirror nucleus of ^{11}N. Taking this as a starting point, we assume that the observed levels in ^{11}N are mainly of SP nature. The SP assumption validates the use of a shell-model potential to describe the experimental data of ^{11}N.

A. Analysis of the three lowest levels in ^{11}N

The ^{11}N states are all in the continuum and the aim of the analysis was to obtain I^{π} and other resonance parameters as it can be done in the framework of the optical model. Because of the absence of other scattering processes than the elastic scattering channel, no imaginary part is included in the potential. The potential has a common form consisting of a Woods-Saxon central potential and a spin-orbit term with the form of a derivative of a Woods-Saxon potential. The Woods-Saxon (ls) term has the usual parameters $V_0(V_{ls})$, $r_0(r_{ls})$, and $a_0(a_{ls})$ for well depth, radius, and diffusity, respectively. Centrifugal and Coulomb terms were also included in the potential. The Coulomb term has the shape of a uniformly charged sphere with radius r_c. The full potential is given in Eq. (16), where μ is the reduced mass of the system and λ_{π} denotes the pion Compton wavelength:

$$V_0=\frac{V_l}{1+e^{(r-R_0)/a_0}}+l\mathbf{s}\frac{V_{ls}(\lambda_{\pi}/2\pi)^2}{a_{ls}} \times\frac{e^{(r-R_{ls})/a_{ls}}}{(1+e^{(r-R_{ls})/a_{ls}})^2}+\frac{l(l+1)\hbar^2}{2\mu r^2}+V_c, \qquad (16)$$

$$V_c=\begin{cases}\dfrac{zZ}{2}\dfrac{e^2}{4\pi\epsilon_0 R_c}\left(3-\dfrac{r^2}{R_c^2}\right): & r<R_c,\\ \dfrac{zZe^2}{r}: & r>R_c,\end{cases}$$

$$R_0=r_0A^{1/3},\quad R_c=r_cA^{1/3},\quad R_{ls}=r_0A^{1/3}.$$

TABLE I. The sets of potential parameters used to obtain the best fits of the experimental data, and the resulting resonance parameters. $V_{ls}=5.5$ MeV is kept the same in all fits. The change of this parameter gave only mirror modifications. The parameter b given in the descriptions below is the value used in $f(E)=b/(4.5\text{-}E)$. (a) $r_0=1.2$ fm, only varying V_l ($b=1.25$). (b) No level inversion ($b=1.25$). (c) The best fit to the data, $r_0=1.4$ fm and varying a and V_l ($b=1.25$). (d) $r_0=1.2$ fm, varying a and V_l ($b=2.4$). (e) The parameters used in Ref. [4] ($b=0$). (f) The parameters used to obtain the widths in the single particle limit.

	Potential parameters				Resonance	
	V_l (MeV)	r_0, r_{ls}, r_c (fm)	a_0 (fm)	a_{ls} (fm)	E_r (MeV)	Γ_r (MeV)
			(a)			
$1s_{1/2}$	−66.066	1.20	0.53	0.53	1.30	1.24
$0p_{1/2}$	−42.336	1.20	0.53	0.53	1.96	0.65
$0p_{3/2}$	−42.084	1.20	0.53	0.53	1.06	
$0d_{3/2}$	−78.792	1.20	0.53	0.53	4.40	0.90
$0d_{5/2}$	−64.092	1.20	0.53	0.53	3.72	0.61
			(b)			
$1s_{1/2}$	−45.360	1.40	0.65	0.30	1.70	3.49
$0p_{1/2}$	−33.474	1.40	0.28	0.30	1.11	0.11
$0p_{3/2}$	−32.340	1.40	0.53	0.30	−1.22	
$0d_{3/2}$	−58.086	1.40	0.53	0.30	4.45	1.23
$0d_{5/2}$	−45.570	1.40	0.35	0.30	3.75	0.60
			(c)			
$1s_{1/2}$	−47.544	1.40	0.65	0.30	1.27	1.44
$0p_{1/2}$	−31.500	1.40	0.55	0.30	2.01	0.84
$0p_{3/2}$	−32.592	1.40	0.53	0.30	−1.33	
$0d_{3/2}$	−57.960	1.40	0.53	0.30	4.5	1.27
$0d_{5/2}$	−45.570	1.40	0.35	0.30	3.75	0.60
			(d)			
$1s_{1/2}$	−56.280	1.20	0.75	0.30	1.32	1.76
$0p_{1/2}$	−42.420	1.20	0.55	0.30	2.14	0.88
$0p_{3/2}$	−42.210	1.20	0.53	0.30	−1.33	
$0d_{3/2}$	−78.960	1.20	0.53	0.30	5.0	1.39
$0d_{5/2}$	−62.874	1.20	0.50	0.30	3.79	0.59
			(e)			
$1s_{1/2}$	−66.066	1.20	0.53	0.53	1.30	1.24
$0p_{1/2}$	−42.084	1.20	0.53	0.53	2.04	0.72
$0p_{3/2}$	−42.084	1.20	0.53	0.53	−1.06	
$0d_{3/2}$	−64.092	1.20	0.53	0.53	9.87	4.53
$0d_{5/2}$	−64.092	1.20	0.53	0.53	3.72	0.61
			(f)			
$1s_{1/2}$	−46.074	1.40	0.70	0.30	1.27	1.56
$0p_{1/2}$	−30.492	1.40	0.70	0.30	2.01	1.09
$0p_{3/2}$	−32.550	1.40	0.53	0.30	−1.31	
$0d_{3/2}$	−57.960	1.40	0.53	0.30	4.50	1.27
$0d_{5/2}$	−42.378	1.40	0.70	0.30	3.75	1.08

As a starting point, standard values of the potential parameters were chosen [21] and the well depths were varied separately for each partial wave ($l=0,1,2$), see Table I(a). The cross section of the experimental data at 180° was found to be larger than predicted by the potential model. As can be seen in the experimental spectrum, Fig. 3, there is substantial

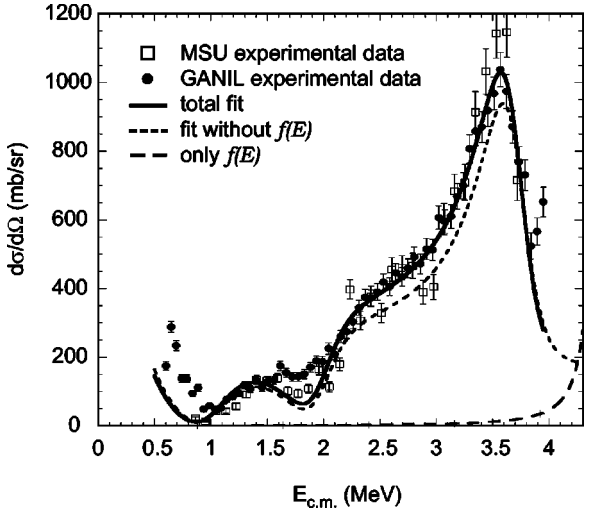

FIG. 4. Experimental excitation function of ^{11}N together with the best fit from the SP-model program. The energy is given as excitation energy of ^{11}N. The fit is made using a potential with parameters shown in Table I(c). The underestimation of the cross section around 1.8 MeV is the only failure of the potential model. This part is better described when the influence of higher resonances is taken into account, see Fig. 9.

amount of cross section above 4 MeV, indicating additional resonances in this energy region.

The underestimation of the potential model can thus be attributed to influence of higher lying resonances. To simulate the presence of those highly excited states, an amplitude f was added to the amplitude calculated from the potential model. The form of this extra amplitude was $f=b/(E_0-E)$ where E_0 was taken as a constant (4.5 MeV) and b was used as a parameter. As is seen in Fig. 4, the introduced amplitude is small in comparison with the measured cross sections, but it nonetheless was useful in the fitting procedure. A more sophisticated way to include the influence of higher resonances is to use an R-matrix procedure, and some attempts in this way were also made, see Sec. IV B.

The best fit for conventional parameters values, only varying V_l is obtained for the level ordering $1s_{1/2}$, $0p_{1/2}$, and $0d_{5/2}$, and the corresponding parameters are given in Table I(a). The curve resulting from these parameters does not differ significantly from the one obtained using the parameter set Table I(c).

A potential with conventional parameters and the same well depth for all l will generate single particle levels in the order $0p_{1/2}$, $1s_{1/2}$, and $0d_{5/2}$ above the $0p_{3/2}$ subshell. However, all attempts to describe the experimental data keeping this ordering of the levels failed. A typical example of a calculated excitation function with this level sequence is shown in Fig. 5, with parameters in Table I(b). This result is not surprising when considering the well known level inversion in ^{11}Be.

For the potential in Table I(c), the cross section of each partial wave is shown in Fig. 6 together with the total calculated curve. Comparing the partial cross sections with the total cross section, it is clear that interference between the partial waves determine the shape of the total curve. The

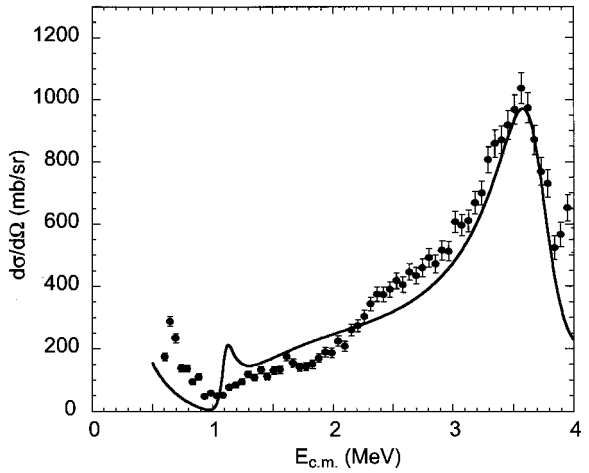

FIG. 5. A typical fit of the experimental data when the $\frac{1}{2}^-$ state is assumed to be the ground state of ^{11}N. It is evident that the excitation function is not well described. Putting the p state this low makes it too narrow, at the same time as the s state becomes very broad since it is now well above the Coulomb barrier.

corresponding phase shifts are shown in Fig. 7. The most common definition of resonance energy is where the phase shift δ_l passes $\pi/2$. As is seen in Fig. 7, the phase of the $\frac{1}{2}^+$ resonance, which is the broadest level, does not reach $\pi/2$. Therefore, we have defined the resonance energy as where the partial-wave amplitude calculated at $r=1$ fm has its maximum. The width is defined as the FWHM of the partial wave. One can note that for the $\frac{1}{2}^-$ and $\frac{5}{2}^+$ levels, the same resonance energies are obtained by our definition and $\delta_l=\pi/2$. All attempts to change the resonance spins and parities or the order of the levels resulted in obvious disagreement with the experimental data. We thus conclude that the unambiguous spin-parity assignments for the lowest states in ^{11}N are a $\frac{1}{2}^+$ ground state, a first excited $\frac{1}{2}^-$ level and a $\frac{5}{2}^+$ second excited state. All further fitting procedures were performed with the aim to obtain more exact data on the positions and widths of the resonances.

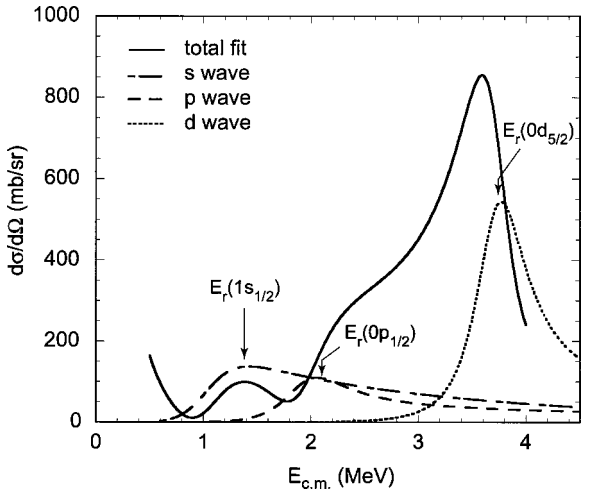

FIG. 6. The partial waves $s_{1/2}$, $p_{1/2}$, and $d_{5/2}$ together with the total calculated excitation function for the best fit to the experimental data [Table I(c)].

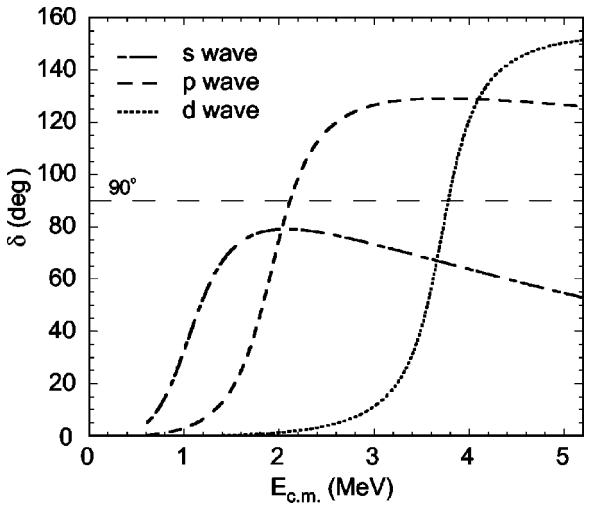

FIG. 7. The phase shifts from the theoretically calculated curve which is the best fit to the experimental data [Table I(c)].

A disadvantage of the potential model is that it produces resonances with single-particle widths. In general, the nature of the states is more complicated and their widths can be smaller than what is predicted by the potential model. To investigate how changing the resonance widths would affect the overall fit, we changed the radius parameter r_0, and fitted new well depths to get the best possible agreement with the data. It was evident that the widths obtained with $r_0=1.4$ fm are too large for the $\frac{1}{2}^-$ and $\frac{5}{2}^+$ resonances, while $r_0=1.0$ fm makes these levels too narrow.

As the $\frac{1}{2}^+$ state is least affected by the change of radius the conclusion for this level is difficult, but the largest obtained width seemed most appropriate. Therefore, the radii parameters r_0, r_{ls}, and r_c were chosen as 1.4 fm, and the well depths and diffusities were varied separately for each l to obtain the best fit of the experimental data up to 4 MeV. An additional argument for choosing the larger radius was the fact that this parameter value gives a good simultaneous description of the mirror pair ^{11}Be and ^{11}N [4]. The curve obtained in this way that agreed best with the experimental excitation function is shown in Fig. 4, and the corresponding potential parameters and resonance energies and widths are shown in Table I(c). For comparison, the values for $r_0=r_{ls}=r_c=1.2$ fm are also given in Table I(d).

The extracted resonance parameters show a remarkable stability against changes in the potential parameter sets, meaning that different sets of parameters that fit the data give similar resonance energies and widths. This is seen in Table I, comparing different sets of parameters. The final energies and widths are listed in Table IV. The error bars include systematic errors and are dominated by a contribution from the spread in results from different parameter sets. Contributions from background subtraction and solid angle corrections will be much smaller than those sources.

The SP reduced widths could be extracted for the three lowest levels where the only possible decay channel is one-proton emission to the ground state of ^{10}C. The values of reduced widths are usually presented as a ratio to the Wigner limit, which serves as a measure of the single particle width [14]. In our case we have a way to give a more exact evaluation of the reduced widths as the ratio of the widths obtained from the shell-model potential that fits the data [Table I(c)] to the widths calculated from a true shell-model potential. These ratios are free from the uncertainties related with different definitions of the level widths. Since the true shell model potential is not known for ^{11}N, and we approximated this potential with the parameters shown in Table I(c).

TABLE II. Reduced widths for the observed states obtained from the ratio of the widths from parameter sets (c) (experimental widths) and (f) (single particle widths) in Table I.

Level I^π	Reduced with Γ_{exp}/Γ_{SP}
$1/2^+$	0.92 ± 0.2
$1/2^-$	0.77 ± 0.2
$5/2^+$	0.56 ± 0.2
$3/2^-$	0.15 ± 0.2

Justification for using this particular set as shell model potential is that it simultaneously reproduces the level positions in both ^{11}Be and ^{11}N and gives a width of the $\frac{1}{2}^+$ state that is larger than for the parameters in Table I(c). The reduced widths obtained in this way are given in Table II.

The potential parameters for the fit of the data at 180° [parameter set (c) in Table I] were used to describe the excitation function obtained by a detector at 12.5° relative to the center of the chamber. The experimental data from this case are shown in Fig. 8 together with the theoretical curve without the scaling amplitude *f*. Comparing the experimental excitation functions in Figs. 4 and 8, rather big differences are seen.

This reflects the fact that the laboratory angle depends on the interaction point in the chamber. The angular range goes from $\theta_{c.m.}=150°$ for protons from higher resonances to $\theta_{c.m.}=93°$ for low energy protons. This is taken into account in the calculation of the excitation function, and from Fig. 8

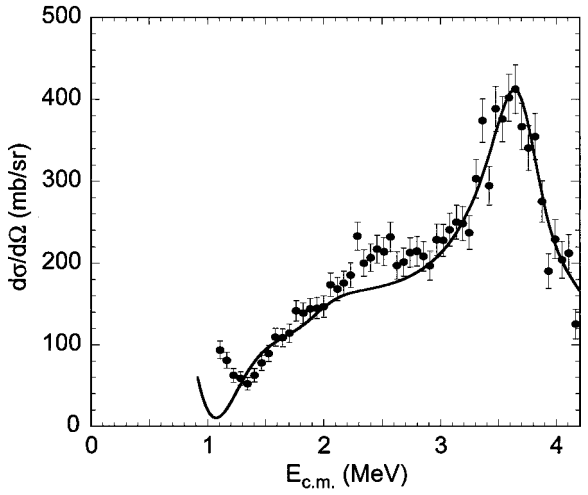

FIG. 8. Experimental spectrum of protons in the detector placed at 12.5° relative to the center of the chamber. The full drawn curve is the result from the potential model using the parameters given in Table I(c).

TABLE III. The resonances used in the simplified *R*-matrix treatment.

	Potential model fit				
	Potential parameters			Resonance	
	V_l (Mev)	$r_0=r_{ls}=r_c$ (fm)	$a_0=a_{ls}$ (fm)	E_r (MeV)	Γ_r (MeV)
$1/2^+$	−66.554	1.2	0.5	1.45	1.56
$1/2^-$	−41.286	1.2	0.6	2.13	0.89
$5/2^+$	−64.801	1.205	0.38	3.74	0.45
	Resonances added in the *R*-matrix fit				
$3/2^+$ [a]				3.94	0.58
$3/2^-$	Mirror of 2.69 MeV level ^{11}Be			4.33	0.27
$(5/2^+)$ [a]	Mirror of 3.41 MeV level ^{11}Be			4.81	0.40
$(7/2^-)$ [a]				5.4	0.25

[a]The parameters for these states are only suggestions which reproduce the observed cross section.

it is evident that the potential model describe the observed changes in the excitation function with angle, a fact which supports our interpretation.

B. Analysis of the full excitation function

In an attempt to investigate the influence of higher lying states on the cross section in the lower part of the experimental spectrum, a simplified *R*-matrix approach was used. For ^{11}Be, about ten levels are predicted in the energy region 2.7 to 5.5 MeV [22], but only four resonances have been experimentally found [20]. The knowledge of the levels in ^{11}N is even more incomplete, and our experimental data are not sufficient for a detailed *R*-matrix analysis. Therefore, the treatment described below was performed rather to outline possible questions than to give definite answers. The analysis was made using the potential model and adding resonances at energies above 4 MeV according to Eq. (17):

$$\frac{d\sigma}{d\Omega}(\theta=180°) = \left| A_{\rm pot} - \frac{i}{2k}\sum_{n_l}^{+}\left[(l+1)(e^{2i\beta_l^+}-1)e^{2i(\phi_l^+ + \sigma_l)}\right] - \frac{i}{2k}\sum_{n_l^-}\left[l(e^{2i\beta_l^-}-1)e^{2i(\phi_l^- + \sigma_l)}\right]\right|^2 . \quad (17)$$

Two known levels in ^{11}Be (2.69 MeV, $\Gamma=200$ keV and 3.41 MeV, $\Gamma=125$ keV) were taken into account. The energy of those resonances in ^{11}N were determined by calculating the Coulomb differences between the mirror nuclei using the potential model. To fit the experimental data, the resonance energies were varied around the value determined from the Coulomb-energy calculation. The values finally used in the *R*-matrix fit are shown in Table III. Again, the superscript $\pm$ denotes states with $j=l\pm\frac{1}{2}$. $A_{\rm pot}$ is the potential model amplitude at 180°, using the potential in Eq. (16).

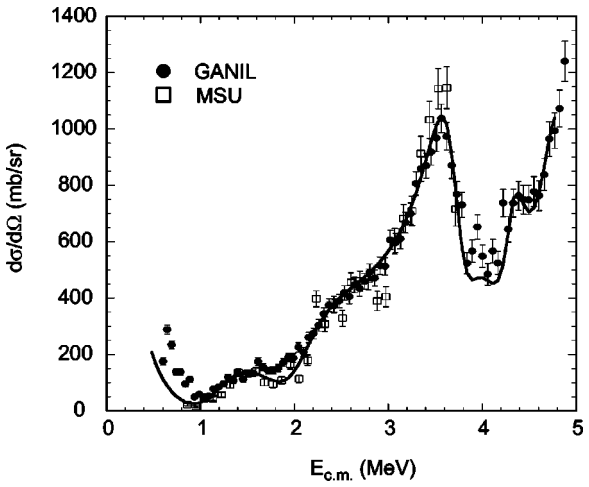

FIG. 9. The fit of the potential model with added resonances. The full drawn curve includes the two known resonances in ^{11}Be plus a broad $\frac{3}{2}^+$ level around 4 MeV and a high-spin state at 5.4 MeV, which gives a good description of the full excitation function up to 4.7 MeV. Especially it should be noted that the theoretical curve now better reproduces the data at 1.6–2.0 MeV.

The resonance phase is $\beta_l^{\pm}$, $n_l^{\pm}$ is the number of resonances, while $\phi_l^{\pm}$ stands for the phase relative to the hard sphere scattering and σ_l is the Coulomb phase of wave *l*. The estimates of the widths of these states in ^{11}N are based on the known widths of the analog states in ^{11}Be. Inclusion of these states already accounts for the missing cross section up to 3.7 MeV, but the part above 3.7 MeV is still underestimated.

In particular, the energy region around 1.8 MeV is now better reproduced, indicating that interference of higher lying states indeed give the cross section that is not reproduced by the potential model in this region. Inclusion of a $3/2^+$ state at 3.94 MeV and a high-spin state improves the description also at energies above 4 MeV, as is seen in Fig. 9. The parameters for the potential and included resonances are given in Table III. The conclusion drawn from comparing the results in Tables I and III is that the positions and widths obtained using only the potential model are rather insensitive to the inclusion of higher states, which only modifies the absolute cross section.

Of the three resonances included in the calculations, only the one at 4.33 MeV is distinctly seen in the excitation function, see Fig. 9. Its position corresponds to the $\frac{3}{2}^-$ state at 2.69 MeV in ^{11}Be within 150 keV, and the cross section supports a spin of $\frac{3}{2}$ for this resonance. The obtained width of 270 keV also agrees with the width of the 2.69 MeV level in ^{11}Be if decay by a $l=1$ proton is assumed. We thus conclude that the narrow resonance at 4.33 MeV in ^{11}N is the mirror of the 2.69 MeV state in ^{11}Be, both having $I^\pi=\frac{3}{2}^-$. The other resonances above 4 MeV are introduced in order to reproduce the cross section at higher energies. The experimental data is not sufficient to give conclusive determination of any parameters of these states, but the existence of resonances above 4.4 MeV is necessary to reproduce the measured cross section.

TABLE IV. A summary of all experimental and theoretical results on ^{11}N. E_r and Γ_r denote the resonance energy and the width of the resonance, respectively. The error bars in this work include the systematic errors (25 keV in the c.m. frame) as well as the spread in results obtained for different potential parameters that all fit the data.

Ref.	$\frac{1}{2}^+$		$\frac{1}{2}^-$		$\frac{5}{2}^+$	
	E_r	Γ_r	E_r	Γ_r	E_r	Γ_r
			Experimental papers			
This work	$1.27^{+0.18}_{-0.05}$	1.44 ± 0.2	$2.01^{+0.15}_{-0.05}$	0.84 ± 0.2	3.75 ± 0.05	0.60 ± 0.05
[13]			2.24 ± 0.1	0.74 ± 0.1		
[23]			2.18 ± 0.05	0.44 ± 0.08	3.63 ± 0.05	0.40 ± 0.08
[24][a]	1.45 ± 0.40	>0.4	2.24 ± 0.1	0.74 ± 0.1		
			Theoretical papers			
[35][a]	1.54	0.62	2.24 ± 0.1	0.74 ± 0.1	3.74	0.3
[25]	1.60 ± 0.22	$2.1^{+1.0}_{-0.7}$	2.49	1.45	3.90	0.88
[36][b]	1.4	1.31	2.21	0.91	3.88	0.72
[31]	1.1	0.9	1.6	0.3	3.8	0.6
[37]	1.2	1.2	2.1	1.0	3.7	1.0

[a]For the $\frac{1}{2}^-$ state the results are from [13].

[b]The results obtained with $r_0=1.45$ fm are presented.

V. DISCUSSION

A. The three lowest resonances in ^{11}N

Table I presents the parameters used in different fits of the deduced excitation function in the $^{10}C+p$ system. The fits were all made under the assumption of three low-lying resonances. From these data we conclude that the three lowest states in ^{11}N have $I^\pi=\frac{1}{2}^+$, $\frac{1}{2}^-$, and $\frac{5}{2}^+$. This is the first time all these states are identified in one single experiment. However, there have been indications of them in other reaction experiments. In the pioneering work on ^{11}N by Benenson *et al.* [13], where the ^{14}N(^{3}He,^{6}He) reaction was studied, it was proposed that the resonance observed at 2.24 MeV ($\Gamma=740$ keV) was a $\frac{1}{2}^-$ state. This conclusion was based on the reaction mechanism in their experiment. Our data confirms this result and both position and width are within the experimental errors of the two experiments. The difference may probably be attributed to different approaches in extracting the resonance parameters. In a recent paper by Lepine-Szily *et al.* [23], a state at 2.18 MeV was observed and interpreted as a $\frac{1}{2}^-$ state, but with a width that was considerably narrower than in our work or that of Ref. [13].

The state at 1.27 MeV, which we interpret as a $\frac{1}{2}^+$ state, could not be seen in the two experiments in Refs. [13], [23], as the selected reactions quench the population of this state considerably. It could, however, be observed in an experiment performed at MSU where Azhari *et al.* [24] studied proton emission from ^{11}N produced in a ^{9}Be(^{12}N,^{11}N) reaction. They found indications of a double peak at low energies and by fixing the upper part of it to the parameters from Ref. [13] they arrived at an excitation energy of 1.45 MeV.

The $\frac{5}{2}^+$ (3.75 MeV) state was discussed in Ref. [4]. The experiment presented in Ref. [23] showed a state at 3.63 MeV with a width about 400 keV. The position of the resonance is close to ours but again the width is smaller in Ref. [23].

As well as for the $\frac{1}{2}^+$ and $\frac{1}{2}^-$ states, the spin value for the $\frac{5}{2}^+$ resonance does not leave any doubt that it is the mirror state of the $\frac{5}{2}^+$ level at 1.78 MeV in ^{11}Be ($\Gamma=100$ keV). The potential model with the parameters used for ^{11}N and given in Table I(c) agrees very well for the width while the excitation energy becomes 1.63 MeV. Still we consider this as an additional support for our interpretation.

Fortune *et al.* [25] have predicted the splitting between $0d_{5/2}$ and $1s_{1/2}$ states in ^{11}N from the systematics of this energy difference for light nuclei, mainly assuming isobaric spin conservation. Their results can therefore be considered as a direct extrapolation of experimental data. The energy difference obtained in our work ($\Delta E=2.48$ MeV) is close to the prediction of 2.3 MeV in Ref. [25]. The energy difference between the $1s_{1/2}$ and $0p_{1/2}$ was calculated using the complex scaling method in Ref. [26] and the value of 830 keV agrees with our data which give 740 keV.

B. Resonances above 4 MeV

We interpret the structure around 4.3 MeV as due to a sharp resonance in ^{11}N, which is the mirror state of the 2.69 MeV level in ^{11}Be, Table III. Several different experiments (see, for example, Ref. [22]) give the spin-parity for this ^{11}Be level as $\frac{3}{2}^-$. The negative parity is well established from measurements of the ^{11}Li β decay [27–29], and by measurements of the ^{9}Be$(t,p)^{11}$Be reaction [22]. There is also good agreement between the Cohen-Kurath prediction for the spectroscopic factor and the reduced single particle widths of these mirror states. We found very good agreement between the widths if the states undergo nucleon decay with $l=1$ ($j=\frac{3}{2}$). If the states decay with orbital momentum, $l=2$ ($j=\frac{3}{2}$), the state in ^{11}N will be at least twice as broad, and in the case of $l=3$ ($j=\frac{5}{2}$) it would be at least 3 times broader. Also, for $l=3$ the reduced single particle width will be too large, contradicting [30]. Using the simplified *R*-matrix ap-

proach, the position of the $\frac{3}{2}^-$ level was determined as 4.33 MeV. The observed cross section for the population of this state is also in accordance with a $\frac{3}{2}^-$ assignment. The calculations further indicate that about one third of the width of the 4.33 MeV state is due to the proton decay to the first excited state in ^{10}C. Even a small branch of this decay results in a large reduced width. This indicates a large coupling of $\frac{3}{2}^-$ state to the first excited state of the core, as was recently predicted by Descouvemont [31]. In Ref. [4] we proposed a different structure for the $\frac{3}{2}^-$ state (two particles in the $1s$ state) because preliminary treatment resulted in a too small width (70 keV) for the state.

In the present experiment there is an experimental cutoff at 5.4 MeV (see Fig. 3) and the excitation function increases towards this high-energy end. This is most likely due to higher-lying states but we cannot make any assignments for them based on our data. However, the authors [24] had to introduce a broad ($\Gamma = 500-1000$ keV) state in the energy region around 4.6 MeV to explain the spectrum from ^{11}N decay. They proposed the broad state to be a $\frac{3}{2}^-$ state. Our data show that the $\frac{3}{2}^-$ state in ^{11}N is rather narrow, and therefore another state has to be assumed in order to explain the data in Ref. [24]. This is also a justification for the inclusion of the $\frac{3}{2}^+$ resonance is our R-matrix fit.

Various theoretical calculations (for recent references see Ref. [32]) have attempted to reproduce the level sequence in ^{11}Be. Most models emphasize the role of coupling between the valence neutron and the first excited 2^+ state in ^{10}Be in generating the parity inversion. It is well known that model assumptions influence the wave functions more than their energy eigenvalues and thus models giving the correct level sequence predict very different core excitation admixtures. For the ground state in ^{11}Be, the admixtures given by theoretical calculations vary from 7% [31,33] to 75% [34]. Theoretical results are frequently compared to spectroscopic factors obtained from nucleon transfer reactions. The single-particle spectroscopic factors for ^{11}Be have been obtained from ^{10}Be(d,p) reactions [30]. Even if the theory of stripping reactions is very well developed, many parameters are involved in the extraction of these results from the data. Evaluating single-particle nucleon widths using a potential model involves fewer parameters. For the lowest states of ^{11}N we obtained the reduced widths given in Table II. For the $s_{1/2}$ state we have a reduced width of ≈ 1 which, taking the 15% experimental error in the width into account, indicates that no large core-excitation admixtures are needed to describe the ground states of ^{11}N and ^{11}Be.

VI. SUMMARY

The excitation function in the ^{10}C$+p$ system has been studied using elastic resonance scattering. The low-energy part was analyzed in a potential model while the high-energy part was described in a simplified R-matrix approach. The ground state and the first two excited states in the unbound nucleus ^{11}N was found to have the spin-parity sequence of $\frac{1}{2}^+$, $\frac{1}{2}^-$, and $\frac{5}{2}^+$ which is identical to that found in its mirror partner ^{11}Be. A narrow $\frac{3}{2}^-$ state at 4.33 MeV was identified as the mirror state of the 2.69 MeV state in ^{11}Be. The energies and widths of the observed states are listed in Table IV. The agreement among experiments as well as between our results and theoretical calculations are very satisfactory.

The quasistationary character of ^{11}N states was used to evaluate the reduced single-particle widths for the identified states. This result indicates small coupling between the valence nucleon in the ground state ^{11}N and the first excited 2^+ state in ^{10}C, and the same conclusion should be valid for ^{11}Be. The experimental technique to use elastic-resonance scattering with radioactive beams has proven to be a very efficient tool for investigations beyond the dripline.

ACKNOWLEDGMENTS

The authors thank Professor M. Zhukov and Professor F. Barker for valuable discussions. The work was partially supported by the National Science Foundation under Grant No. PHY95-28844. The work was also partly supported by a grant from RFBR. S.B. acknowledges the support of the REU program under Grant No. PHY94-24140.

[1] K. P. Artemov *et al.*, Yad. Fiz. **52**, 634 (1990) [Sov. J. Nucl. Phys. **52**, 408 (1990)].
[2] V. Z. Goldberg *et al.*, Yad. Fiz. **60**, 1186 (1997) [Phys. At. Nucl. **60**, 1061 (1997)].
[3] V. Z. Goldberg and A. E. Pakhomov, Yad. Fiz. **56**, 31 (1993) [Phys. At. Nucl. **56**, 17 (1993)].
[4] L. Axelsson, *et al.*, Phys. Rev. C **54**, R1511 (1996).
[5] R. Coszach *et al.*, Phys. Rev. C **50**, 1695 (1994).
[6] M. Benjelloun *et al.*, Nucl. Instrum. Methods Phys. Res. A **321**, 521 (1992).
[7] B. Jonson and K. Riisager, Philos. Trans. R. Soc. London, Ser. A **356**, 2063 (1998).
[8] R. Anne *et al.*, Phys. Lett. B **304**, 55 (1993).
[9] F. M. Nunes, I. J. Thompson, and R. C. Johnson, Nucl. Phys. **A596**, 171 (1996).
[10] D. J. Millener, J. W. Olness, E. K. Warburton, and S. S. Hanna, Phys. Rev. C **28**, 497 (1983).
[11] I. Talmi and I. Unna, Phys. Rev. Lett. **4**, 469 (1960).
[12] H. Sagawa, B. A. Brown, and H. Esbensen, Phys. Lett. B **309**, 1 (1993).
[13] W. Benenson *et al.*, Phys. Rev. C **9**, 2130 (1974).
[14] G. Breit and E. Wigner, Phys. Rep. **49**, 519 (1936).
[15] P. E. Hodgson, E. Gadioli, and E. Gadioli Erba, *Introductory Nuclear Physics* (Oxford Science, Oxford, 1997).
[16] R. A. Laubenstein and M. J. W. Laubenstein, Phys. Rev. **84**, 18 (1951).
[17] J. B. Marion and F. C. Young, *Nuclear Reaction Analysis (Graphs and Tables)* (North-Holland, Amsterdam, 1968).
[18] D. L. Auton, Nucl. Phys. **A157**, 305 (1970).
[19] H. L. Jackson and A. I. Galonsky, Phys. Rep. **89**, 370 (1953).
[20] F. Ajzenberg-Selove, Nucl. Phys. **A506**, 1 (1990).
[21] K. S. Krane, *Introductory Nuclear Physics* (Wiley, New York, 1988).

[22] G.-B. Liu and H. T. Fortune, Phys. Rev. C **42**, 167 (1990).
[23] A. Lépine-Szily *et al.*, Phys. Rev. Lett. **80**, 1601 (1998).
[24] A. Azhari *et al.*, Phys. Rev. C **57**, 628 (1998).
[25] H. T. Fortune, D. Koltenuk, and C. K. Lau, Phys. Rev. C **51**, 3023 (1995).
[26] A. Aoyama, N. Itagaki, K. Kato, and K. Ikeda, Phys. Rev. C **57**, 975 (1998).
[27] N. Aoi *et al.*, Nucl. Phys. **A616**, 181c (1997).
[28] D. J. Morrisey *et al.*, Nucl. Phys. **A627**, 222 (1997).
[29] I. Mukha *et al.* (unpublished).
[30] B. Zwieglinski, W. Benenson, and R. H. G. Robertson, Nucl. Phys. **A315**, 124 (1979).
[31] P. Descouvemont, Nucl. Phys. **A615**, 261 (1997).
[32] S. Fortier *et al.*, Phys. Lett. B **461**, 22 (1999).
[33] N. Vinh Mau, Nucl. Phys. **A592**, 33 (1995).
[34] I. Ragnarsson, in Proceedings of the International Workshop on The Science of Intense Radioactive Beams, LA-11964-c, Los Alamos, 1990 (unpublished), p. 199.
[35] R. Sherr, Coulomb shifts in $A=11$ quartet (IMME) (private communication).
[36] F. C. Barker, Phys. Rev. C **53**, 1449 (1996).
[37] S. Grévy, O. Sorlin, and N. Vinh Mau, Phys. Rev. C **56**, 2885 (1997).